Materials Science & Engineering C 94 (2019) 608–618

Contents lists available at ScienceDirect

Materials Science & Engineering C

journal homepage: www.elsevier.com/locate/msec

Multifunctional magnetic cargo-complexes with radical scavenging properties

Ana-Lacramioara Lungoci[a], Ioana-Andreea Turin-Moleavin[a], Andreea Corciova[b], Cornelia Mircea[b], Adina Arvinte[a], Adrian Fifere[a,*], Narcisa Laura Marangoci[a], Mariana Pinteala[a]

[a] Centre of Advanced Research in Bionanoconjugates and Biopolymers Department, "Petru Poni" Institute of Macromolecular Chemistry, 41A Grigore Ghica-Voda Alley, 700487 Iasi, Romania
[b] Faculty of Pharmacy, "Grigore T. Popa" University of Medicine and Pharmacy, 16 Universitatii Street, RO-700115 Iasi, Romania

ARTICLE INFO

Keywords:
Magnetic nanoparticles
Antioxidant activity
Free radical scavengers
Protocatechuic acid
Cyclodextrin inclusion complex

ABSTRACT

Core-shell magnetic nanoparticle synthesis offers the opportunity to engineering their physical properties for specific applications when the intrinsic magnetic properties can be associated with other interesting ones.

The purpose of this study was to design, synthesize, and characterize core-shell magnetic nanoparticles that mimic superoxide dismutase activity offering the possibility of guidance and therapeutic action. We proposed, for the first time, the synthesis and characterization of the nanocarriers comprised of magnetite nanoparticles functionalized with branched polyethyleneimine of low molecular weight (1.8 kDa) permitting the loading of the protocatechuic acid or its inclusion complex with anionic sulfobutylether-β-cyclodextrin for active drug delivery, in order to combine the useful properties of the magnetite and the protocatechuic acid antioxidant effect. NMR and DSC analyses confirmed the formation of the inclusion complex between sulfobutylether-β-cyclodextrin and protocatechuic acid, while structural and compositional analyses (FT-IR, TEM, XRD) revealed the synthesis of the multifunctional magnetic systems. Due to the possibility of being formulated as blood system injectable suspensions, antioxidant activity (using DPPH test) and cytotoxicity (using MTS assay on normal human dermal fibroblasts cells) were also measured, showing adequate properties to be used in biomedical applications. Moreover, we proposed a nanocarrier that would be able to load unstable active principles and with very low solubility in biological fluids to increase their biological ability.

1. Introduction

In the last decade, the knowledge about reactive oxygen species (ROS) and their importance in human health have increased considerably. ROS are chemically interesting and biologically ambivalent, extremely reactive species due to their unpaired electrons. They can come from natural metabolic processes (phagocytosis, mitochondrial activity, hepatic detoxification) or may derive from environment (cigarette smoke, pollution, processed food and therapeutic agents). The pathway from molecular oxygen to superoxide anion, hydrogen peroxide and finally hydroxyl radicals goes through enzymes, such as superoxide dismutase and glutathione peroxidase. Their effects in biological media can be both beneficial and damaging. In low quantities they can act as signalling molecules, alerting the immune function, whereas the high levels induce oxidative stress, which can damage macromolecules and trigger the pathogenesis of many diseases [1]. The involved systems are respiratory, renal, vascular (endothelial dysfunctions) and the pathologies can be diabetes, hypertension, Parkinson's disease and ischemia. The oxygen in ROS can initiate aggressive oxidation reactions inside cells or at the surface of cell membranes, damaging DNA, oxidizing unsaturated fatty acids from lipids or amino acids from proteins [2]. Antioxidants (enzymatic or non-enzymatic) can inhibit these dangerous oxidative processes by maintaining a redox balance.

When a therapeutic approach is under consideration, two important things must be taken into account: one is the importance to maintain an antioxidants adequate level on the interest site, like the endothelial vessel affected by atherosclerosis; the second important think is the long term stability and constant release of the therapeutic agent.

Taking into account the combined properties of the free radical scavengers of the natural antioxidants [3] and the thermic effect of the magnetite nanoparticles (MNP) in alternating magnetic field, one interesting proposal is to implement a magnetic nano-entity able to intravascularly deliver anti-oxidants in a pharmacologically controlled

* Corresponding author.
E-mail address: fifere@icmpp.ro (A. Fifere).

https://doi.org/10.1016/j.msec.2018.10.013
Received 28 February 2018; Received in revised form 31 July 2018; Accepted 2 October 2018
Available online 04 October 2018
0928-4931/

and spatially guided manner. In this way it is possible to simultaneously reduce ROS and eradicate modified cells from cancer tumours by hyperthermia, which relies on the properties of ferromagnetic iron oxide core of the nanoparticles. To attain this aim a nano-sized cargo-complex having a magnetic core and polyelectrolyte - based shell able to load and to deliver precise amounts of natural antioxidants as free radical scavengers can be taken into consideration.

The fact that a wide range of antioxidants are organic acids, suggested the idea that they could be charged in layers of organic cationic polymers, allowing easy attachment of the antioxidant (bearing carboxylic groups) based on electrostatic interactions or by metal complexation [4]. As many synthetic and natural antioxidants have low water solubility, they are encapsulated in water soluble macrocyclic molecules such as cyclodextrins (CD) [5]. Currently, native and modified cyclodextrins are required in biomedical applications due to their properties, such as good biocompatibility, water solubility and, as the demand is increasingly high, have become low-priced in a large variety of chemical modifications [6]. In this context, modified cyclodextrins with anionic groups may be selectively absorbed in cationic polyelectrolyte shell of the nanoparticles based on electrostatic driven forces, in which case the cyclodextrin may play the role of host for low soluble antioxidant by forming host-guest inclusion compounds.

As antioxidant compound can be used a natural phenolic acid as 3,4-dihydroxybenzoic acid, also named protocatechuic acid (PCA), originated usually in traditional Chinese herbal medicines. Apparently, many of the pharmacological effects of PCA are in close relation with the antioxidant properties. In this context, the antioxidant activity and antioxidant mechanism of PCA was recently highlighted by the Xican Li et al. [7] using *in vitro* antioxidant assays. Therefore, they reported that PCA shows more antioxidant activity *in vitro* than Trolox. The authors suggested that PCA can act as a scavenger of free radicals by mechanisms such as donating a hydrogen atom or an electron.

PCA was used, also, as a stabilizer of magnetic nanoparticles in water, when the functionalization of the magnetic nanoparticles was done by a ligand exchange reaction [8]. The resulted nanoparticles presented a good biocompatibility, high saturation magnetization and a good potential as contrast agent in Magnetic Resonance Imaging (MRI). Later, the PCA was used as a template for polymeric coating of magnetite nanoparticles, increasing stability in physiological media and improving pharmacokinetic properties by tailoring drug loading capacity and release behavior [9].

Most of the time, the success of magnetite nanoparticles was closely linked to their physical properties, generated by the presence of a permanent magnetic field, which make them useful in applications as contrast agents in MRI [10] or as therapeutic agents in hyperthermia treatment [11]. Along with their covering with polymers to increase their colloidal stability in solution, it has opened a wide range of applications as in targeted and controlled drug delivery and a variety of other theranostic applications [12].

Moreover, core-shell magnetic nanoparticle synthesis offers the opportunity to engineering their physical properties for specific applications when the intrinsic magnetic properties can be associated with other interesting ones (ex. chemical or biological purposes) when the surface allows the presence of drugs, active chemical agents (like polymer initiators) or redox substances [13–15]. Hence, the loading of core-shell magnetic nanoparticles with natural antioxidants could combine the magnetic properties of the core with the radical scavenging characteristics of the drugs, offering both the possibility of guidance and therapeutic action. In this context, a potential example would be an atherosclerotic artery, where restenosis after percutaneous coronary intervention can be avoided by reducing local oxidative stress levels.

The purpose of this study was to design, synthesize, and characterize core-shell magnetic nanoparticles that mimic superoxide dismutase activity; therefore they are working as a free radical scavenger in a desired place. Specifically, we proposed, for the first time, the synthesis and characterization of the nanocarriers comprised of ferrite nanoparticles functionalized with branched polyethylenimines (PEI, 1.8 kDa) permitting the loading of the protocatechuic acid (PCA) or its inclusion complex with sulfobutylether-β-cyclodextrin (SBEβCD/PCA) for active drug delivery in order to combine the useful properties of the magnetite and the PCA antioxidant effect. It should be pointed out that PEIs of low molecular weight, due to their primary, secondary and tertiary amino groups, ionically interact with anionic polymers and ampholytes at neutral or mildly alkaline values of pH and are accepted for biological interest [16,17].

2. Materials and methods

2.1. Materials

Materials were bought as follows: ferric chloride ($FeCl_3{\cdot}6H_2O$), ferrous chloride ($FeCl_2{\cdot}4H_2O$), 25% ammonium solution, polyethylenimine of 1.8 kDa (PEI), protocatechuic acid (PCA), and 2,2-diphenyl-1-picrylhydrazyl (DPPH), 2,2′-azino-bis (3-ethylbenzothiazoline-6-sulfonic acid diammonium salt (ABTS diammonium salt), and potassium persulfate from Sigma Aldrich; sulfobutylether-β-cyclodextrin sodium salt (SBEβCD) was purchased from Ligand Pharmaceuticals, Inc.; normal human dermal fibroblasts (NHDF) from PromoCell; CellTiter 96® AQ_{ueous} One Solution Reagent, containing a novel tetrazolium compound [3-(4,5-dimethyl-2-yl)-5-(3-carboxymethoxyphenyl)-2-(4-sulfophenyl)-2H-tetrazolium, inner salt; MTS] and an electron coupling reagent (phenazine ethosulfate; PES) from Promega; alpha-MEM medium and 1% Penicillin-Streptomycin-Amphotericin B mixture from Lonza; 10% fetal bovine serum FBS from Gibco.

2.2. Syntheses

Synthesis of loaded conjugates with PCA antioxidant was performed in three steps:

(a) synthesis of MNP by co-precipitation method of Fe^{2+} and Fe^{3+} salts in a molar ratio of 0.5, in water solution at pH of 11–12 [18–20,23];
(b) MNPs were coated with PEI polymer (MPEI) by mixing the components in deionized water at room temperature;
(c) loading of MPEI nanoparticles with PCA and SBEβCD/PCA inclusion complex, named MPEI-PCA and MPEI-SBEβCD/PCA, respectively when PEI cationic polymer is able to easily embed acidic-type natural polyphenol antioxidants.

When SBEβCD/PCA inclusion complex is used, the drug is released in two stages: in the first step the inclusion complex is released from the PEI polymeric coating of the nanoparticle, and in the second step the antioxidant will be released from the SBEβCD cavity in a desired place due to the magnetic properties of the core. It should be mentioned that PCA was included in SBEβCDs cavity to favour its solubility and bioavailability and, also, the absorption of the inclusion complex into the polymeric shell of nanoparticles creates the premises for the possibility of embedding other natural antioxidants in the PEI shell.

2.2.1. Inclusion complexes synthesis (SBEβCD/PCA)

1.84 g (1.29 mmol) of SBEβCD were dissolved in 50 ml deionized water and the solution was kept under stirring, at room temperature, until the solution became clear, than 0.2 g (1.29 mmol) of PCA were added and the solution was stirred until became clear when it was submitted for lyophilization [21,22].

2.2.2. Magnetite nanoparticles (MNP) synthesis

MNP were synthesized by the classical method of co-precipitation [23]. In brief: 10 ml ammonium aqueous solution (25%) were added onto a solution mixture of ferrous and ferric salts, in a molar ratio of 0.5 under nitrogen protection and mechanical stirring at 70 °C and the

colour of the solution starts to be black. The mixture was maintained under mechanical stirring and 70 °C for the other 30 min., after that the temperature was decreased at room temperature and the prepared MNP were magnetically separated and were washed several times with deionized water and ethanol. The MNP were kept in refrigerator as dispersion in dry ethanol. Prior to use, the MNPs were magnetically separated and five times washed with deionized water to remove ethanol traces and MNPs were re-suspended in deionized water to obtain a stock solution.

2.2.3. MNP coating with PEI (MPEI)

From a proper volume of MNPs stock solution, 50 mg MNPs were separated and 10 ml of 10% of 1.8 kDa PEI water solution were added under mechanical stirring. The resulted dispersion was sonicated for 3 min, followed by mechanical stirring for 2 h [24]. Prior to use, MNPs were separated with the help of a permanent magnet and washed five times with deionized water for removing unreacted PEI and were collected with a permanent magnet. After that MPEI magnetite particles were dispersed by sonication for 5 min in deionized water in a concentration of 100 mg/ml.

2.2.4. Loading of PCA antioxidant in the shell of MPEI (MPEI-PCA)

1 ml PCA solution of 10 mg/ml was added onto 1 ml MPEI (50 mg/ml) under mechanical stirring, during 15 min. The resulted suspension was sonicated for 2 min and kept under gentile stirring for 24 h. MPEI-PCA nanoparticles were separated by magnetic decantation and were washed 5 times with 2 ml deionized water each. The washing water (10 ml) was added over the resulting supernatant after particle separation to estimate the amount of PCA not absorbed in the PEI layer. Using the same procedure, nanoparticles were loaded with SBEβCD/PCA inclusion complex (the sample was noted as MPEI-SBEβCD/PCA).

The entrapment efficiency of PCA or SBEβCD/PCA into MPEIs shell was calculated by absorbance reading at 287 nm (using 1 cm quartz cuvettes) of resulted supernatant solution (Fig. 1S, from Supplementary material) by using Eq. (1) [25,26]:

$$\text{Entrappment efficiency (\%)} = 100\frac{\text{total amount of drug} - \text{free amount of drug}}{\text{total amount of drug}} \quad (1)$$

where: total amount of drug and free amount of drug was determined using calibration curves as absorbance at 287 nm *vs.* concentration of free PCA or SBEβCD/PCA (Fig. 2S).

2.3. Methods

2.3.1. Release of antioxidant agent

The PCA release profile of loaded nanoparticles (MPEI-PCA and MPEI-SBEβCD/PCA) was studied in phosphate-buffered saline solution using PBS of pH 7.4. An amount of 30 mg of loaded nanoparticles were placed into dialysis bag with cut off of 12 kDa and it was introduced in 30 ml PBS, under gentile stirring at 37 °C. To determine the concentration of released PCA and its release profile, 2 ml of supernatant was taken out every 30 min., and replaced with 2 ml of fresh buffer solution. 1 ml of supernatant was diluted with 1 ml of PBS and assayed by UV–Vis spectroscopy at 250 nm.

The amount of released PCA antioxidant was determined with the help of calibration curve of PCA (Fig. 2S) and the concentration values being calculated as [27]:

$$C_f' = C_f + \frac{v}{V}\sum_{i=1}^{n} C_{f_{i-1}} \quad (2)$$

where: v is the volume of release media taken out every time and V is the diluted volume subjected to UV–Vis measurements, C_f' is concentration of released drug and C_f is the concentration in the volume V at specific time.

2.3.2. Free radicals scavenger activity by DPPH assay

The antioxidant activity of functionalized magnetite nanoparticles was measured using DPPH (2,2-diphenyl-1-picrylhydrazyl) method [28]. 3 ml methanol solution of DPPH (0.1 mg/ml) was added in each 3 ml suspensions in methanol of MPEI-PCA and MPEI-SBEβCD/PCA conjugates of different concentrations. After 30 min stirring, the absorbance measurements of the samples were taken, using 1 cm quartz cuvettes. The radical scavenging activity was calculated using Eq. (3), taken into consideration the absorbance values at 517 nm of the samples:

$$\%\text{of inhibition} = \frac{Ac - As}{Ac} \times 100 \quad (3)$$

where: *As* is the absorbance of the samples with PCA of different concentrations and formulations and *Ac* is the absorbance of the DPPH solution of 0.05 mg/ml.

2.3.3. Free radicals scavenger activity by ABTS assay

The antioxidant activity was measured using ABTS method [29]. ABTS cation radical reagent was prepared by mixing 19.2 mg ABTS diammonium salt solved in 2.5 ml distilled water with the aqueous solution of 3.31 mg potassium persulfate and let to stand in the dark, at room temperature. After 24 h, the mixture is diluted with ethanol to a solution with absorbance 0.7 ± 0.02 at 734 nm. 0.025 ml sample solution is mixed with 2.475 ml ABTS cation radical reagent and the absorbance is read up to 6 min at 30 °C. Scavenger activity is calculated according to the Formula (3), where *As* becomes the absorbance of the ABTS cation radical reagent treated with sample solution and *Ac* becomes the absorbance of ABTS cation radical reagent.

The *cell viability test* was carried out *via* the reduction of the 3-(4,5-dimethylthiazol-2-yl)-5-(3-carboxymethoxyphenyl)-2-(4-sulfophenyl)-2H-tetrazolium inner salt MTS reagent, as a function of mitochondrial activity. Cytotoxicity of the three types of nanoparticles (MPEI, MPEI-PCA, MPEI-SBEβCD/PCA) were tested in NHDF cells using the CellTiter 96® AQ_{ueous} One Solution Cell Proliferation Assay [17]. Fibroblasts were expanded and maintained in alpha-MEM medium supplemented with 10% fetal bovine serum and 1% Penicillin-Streptomycin-Amphotericin B mixture (10 K/10 K/25 µg in 100 ml) at 37 °C, 5% CO_2 and humidified atmosphere when NHDF cells were plated in 96-well format (5×10^3 cells/well/100 µl) for 24 h. After the cell adhesion occurred, the media was changed and replaced with solutions in a wide range of treatment concentrations (from 0.39 to 50 µg/ml). Control wells received only cell culture medium. After 44 h of incubation, a volume of 20 µl of CellTiter 96®AQueousOne Solution reagent was added to each well and the plates were incubated for 3 h at 37 °C. The absorbance at 490 nm was recorded with a plate reader (EnSight, PerkinElmer) and the relative cell viability (%) was calculated by [(At − Ab) / (Ac − Ab)] × 100 formula where At = absorbance value of the sample, Ac = absorbance value of the control and Ab = absorbance value of the blank. Eight replicates were measured and the results presented as mean ± standard deviation.

The *nuclear magnetic resonance (NMR)* technics were involved in elucidation of the inclusion compound structures. The NMR spectra have been recorded on a Bruker Avance DRX 400 spectrometer operating at 400.1 MHz for ^{1}H and 100.6 MHz for ^{13}C nuclei.

The Fourier-transform infrared (FTIR) spectra were recorded using a Bruker Vertex 70 FTIR instrument, in transmission mode, in the 400–4000 cm^{-1} range (resolution 2 cm^{-1}, 32 scans), at ambient temperature, in KBr pellet.

X-ray diffraction (XRD) analysis was performed in a Brucker D8 Advance in the range 20–120° with a rate of 3°min^{-1}. Co Kα radiation (λ = 1.5406 Å) was used and the tube operated at 36 kV and 30 mA.

The *hydrodynamic diameter and zeta potential* of the nanoparticles were evaluated using Delsa Nano C Submicron Particle Size Analyzer (Beckman Coulter, Inc., Fullerton, CA). This device is equipped with a laser diode operating at 658 nm. Measurements were made at room

temperature in flow cell for both sizes and zeta potential values; before measurements the solution was dispersed by ultrasonication.

Transmission electron microscopy (TEM) investigations were carried out with a Hitachi High-Tech HT7700 Transmission Electron Microscope operated at a 100 kV accelerating voltage in High-Contrast Mode. The samples were prepared on carbon-coated copper grids with 300-mesh sizes. Microdroplets of the nanoparticles dispersed in water were placed on the grids, and then the solvent was removed under vacuum. Statistical data of the size distributions were carried out with soft Image J by measuring 100 nanoparticles.

Differential scanning calorimetry (DSC) measurements were performed on a DSC 200 F3 Maia device (Netzsch, Germany). Around 4 mg of sample was heated in aluminium crucibles with pierced and pressed shut lids. A heating rate of 10 °C min^{-1} was applied and nitrogen was used as purge gas at a flow rate of 50 ml min^{-1}. The device was calibrated with indium, according to standard procedures.

The voltammetric measurements were performed using AUTOLAB PGSTAT302N electrochemical system from ECO CHEMIE Utrecht, The Netherlands, and a single compartment electrochemical cell of 100 µl PBS 0.1 M or $NaClO_4$ 0.1 M, as specified in each experiment. Cyclic voltammetry (CV) was employed to study the electrochemical behaviour of uncovered or covered magnetite nanoparticles, deposited as adsorbed layer (3 µl) from their aqueous solutions on the screen-printed electrode with a planar configuration, fabricated and purchased from Biosensor Laboratory, University of Florence, Italy. The working carbon-based electrode with a disk shape of 3 mm diameter, the silver reference and carbon counter electrode were symmetrically disposed around working electrode.

Measurement of magnetization was carried out at room temperature with a Vibrating Sample Magnetometer – MicroMag, Princeton Measurements Corporation.

UV–Vis measurements were performed on a Perkin Elmer Inc., USA, apparatus. The emission spectra were measured in the 190–700 nm range for identical sample volumes (3 ml) with the following parameters: slit width 1 nm, scan speed 480 nm/min and data interval 1 nm. The spectra of the samples were measured at room temperature using 1 cm path length quartz cuvettes.

3. Results and discussions

We have proposed a method to obtain, in a reproducible way, surface functionalization of magnetic nanoparticles with PEI of low molecular weight (1.8 kDa) when PEI became cyto-friendly [30], being able to load the PCA or its inclusion complex SBEβCD/PCA by electrostatic interactions (Fig. 1).

3.1. Synthesis and structural characterization of SBEβCD/PCA inclusion complex

The inclusion complex with potential radical scavenger activity (Fig. 1) was obtained by mixing SBEβCD and PCA in a 1/1 molar ratio in deionized water and the clear solution has been processed by freeze drying method. The white powder compound was used without a subsequent separation of unreacted compounds. Structure elucidation of the inclusion compound was achieved by 1D and 2D NMR techniques.

The ^{1}H NMR spectra (Fig. 3S) presents the SBEβCD/PCA inclusion complex in comparison with the chemical shifts of the same protons in its free components. It was observed that all protons signals of the PCA have downfield shifts between 0.06 ppm–0.006 ppm during its complexation, suggesting that PCA was included inside the SBEβCD's cavity in several possible orientations in a dynamic way. In the same manner, SBEβCD's protons have complementary chemical shifts variations, suggesting a cyclodextrin conformational effort in order to adapt the molecular geometry in a supramolecular state of its inclusion compound.

To elucidate in more details the structure of SBEβCD/PCA inclusion complex, ROESY (Rotating frame Overhause Effect Spectroscopy) 2D NMR spectrum was performed (Fig. 4S), providing correlations between different protons that are presented in 1D spectra but frequently difficult to extract. The ROESY 2D NMR spectrum (Fig. 4S) of the SBEβCD/PCA inclusion complex shows intermolecular NOE (Nuclear Overhauser enhancement) cross-peaks between phenolic protons signals of PCA and H3, H5 protons which are located inside the cavity of cyclodextrin. These data do not elucidate the exact position of the PCA inside the cyclodextrin's cavity, suggesting once again a multiple conformer's coexistence [31] but confirms the formation of the SBEβCD/PCA inclusion complex.

DSC is an important technique for confirmation of host–guest type interaction occurrences in the solid state. This interaction is highlighted by the decreasing and dislocation, or complete disappearance of the melting transition temperature of guest molecule after inclusion in the host's cavity [5,21,32]. As indicated in Fig. 2b, the guest molecule (PCA) exhibits an intense melting profile at 205 °C observed for physical mixtures. The DSC curve of the SBEβCD/PCA inclusion complex indicated a significant reduction of the intensity and displacement towards higher temperatures of the melting point as a consequence of PCA thermal protection by the host's cavity (T_m = 217 °C for SBEβCD/PCA), indicating new solid phases formation by complexation [22] (Fig. 2c).The endothermic broad profiles presented in the 75–135 °C interval are due to loss of crystallized water molecules from host's cavity.

Inclusion efficiency of 99.56% was obtained by applying Eq. (3), where ΔH_{ic} is the PCA melting enthalpy in the inclusion complex and ΔH_u is the pure PCA melting enthalpy [33]:

$$\text{Inclusion}\ (\%) = 100\left(1 - \frac{\Delta H_{ic}}{\Delta H_u}\right) \quad (4)$$

3.2. X-ray diffraction of uncovered magnetite nanoparticles (MNP)

X-ray diffraction was performed to confirm the crystalline nature of the magnetite nanoparticles. The diffractogram analysis of the MNP crystalline structure (Fig. 3) shows the main reflection planes by their Miller indices (220), (311), (400), (511) and (440) (see the numbers inserted in Fig. 3) which can be well indexed to the Fe_3O_4 inverse cubic spinel structure [34,35].

3.3. FT-IR study of MPEI, MPEI-PCA and MPEI- SBEβCD/PCA conjugates

The FT-IR spectrum of the MNP (Fig. 4a), the peak at 572 cm^{-1} and the shoulder at 630 cm^{-1} are associated to the stretching vibrations of the Fe—O bond in magnetite crystalline structure [19]. When MNP were covered with PEI polymer, the vibrational bands at 3240 cm^{-1} (shoulder) and 1545 cm^{-1} associated with stretching and bending vibrations of the N—H bonds can be observed in FT-IR spectrum (Fig. 4b). On the other hand, the signals at 1467 cm^{-1} and in the region between 1000 and 1330 cm^{-1} are associated to the stretching vibrations of C—H bonds from PEI.

The FTIR spectrum of PCA (Fig. 4c) shows the vibration bands characteristic of the —COOH groups through the C═O stretching vibration at 1676 cm^{-1} and 1300 cm^{-1} and the bands at 557 cm^{-1} and 942 cm^{-1} attributed to the —OH bending vibrations [36]. The bands at 1467 cm^{-1} and 1528 cm^{-1} are assigned to the stretching mode of the C—C aromatic ring.

The FT-IR spectra of MPEI-PCA (Fig. 4d) and MPEI-SBEβCD/PCA (Fig. 4e) conjugates contain some similarities due to the presence of the PCA characteristic vibrations, registered at 1365 cm^{-1} and 1357 cm^{-1}, assigned to the bending vibrations of the PCA phenolic groups in MPEI-PCA and MPEI-SBEβCD/PCA, respectively. Moreover, the pronounced stretching vibration of the carbonyl group of PCA is visible in

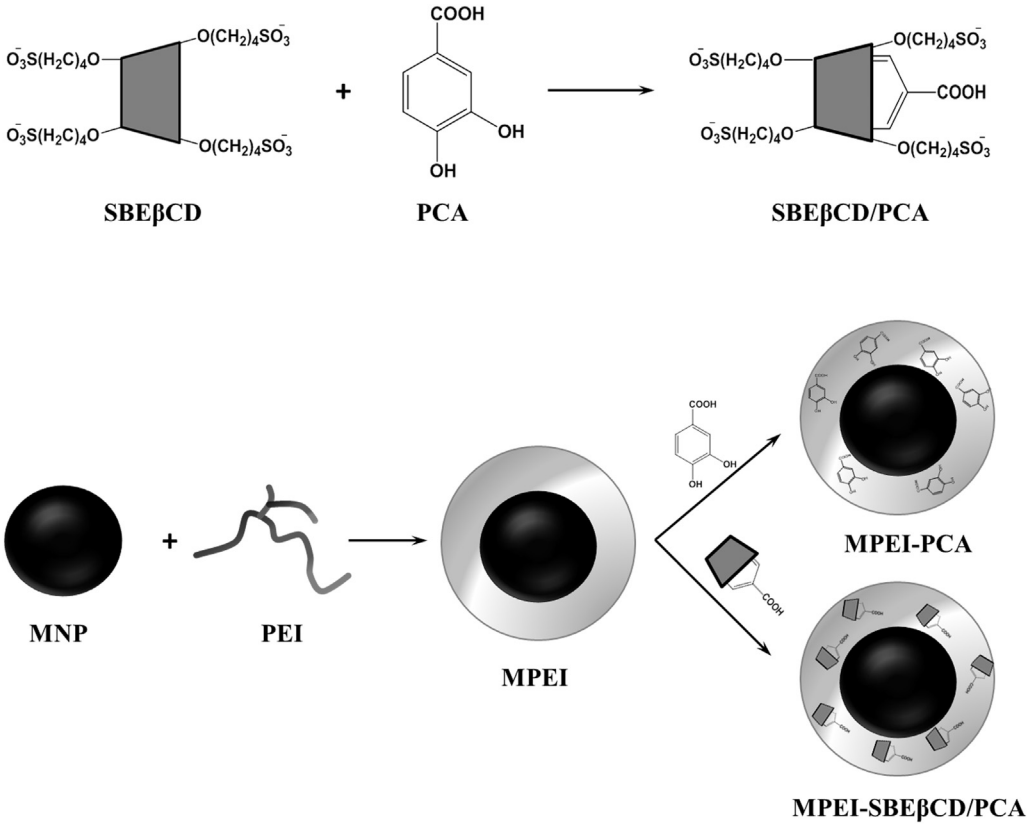

Fig. 1. Schematic representation of SBEβCD/PCA, MPEI-PCA and MPEI-SBEβCD/PCA synthesis.

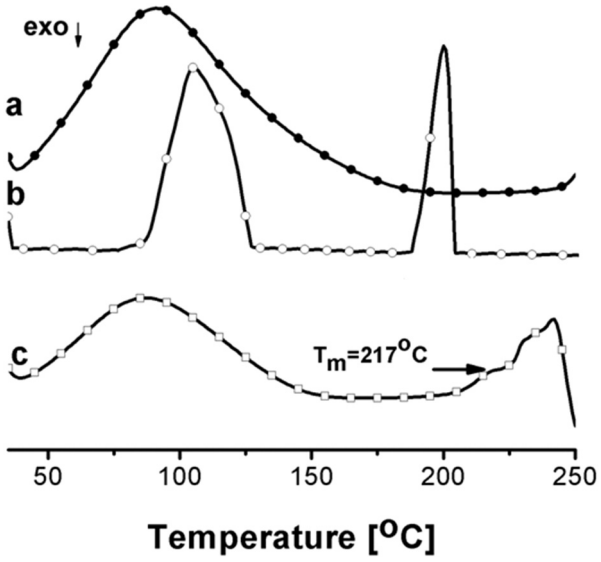

Fig. 2. DSC heating curves of (a) SBEβCD, (b) physical mixture of SBEβCD and PCA, and (c) SBEβCD/PCA.

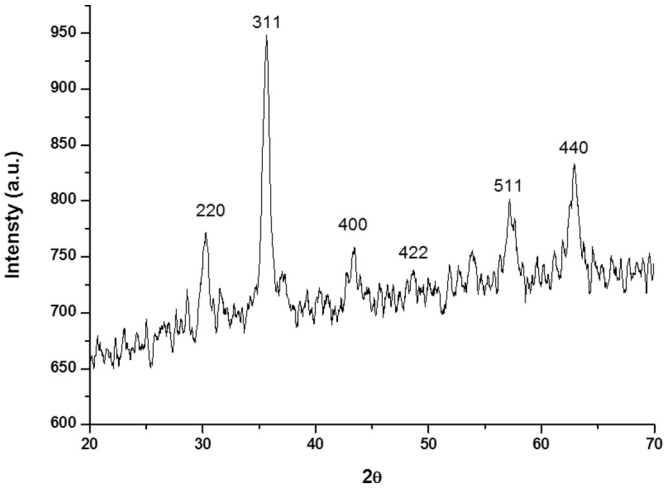

Fig. 3. X-ray diffraction patterns of pure Fe_3O_4 MNP.

1690–1680 cm^{-1} and bending vibrations of −OH carboxylic groups at 942–947 cm^{-1} region of both loaded structures with PCA [37]. It should be mentioned that do exist some differences between the key features of PCA, MPEI-PCA and MPEI-SBEβCD/PCA in FT-IR spectra which are due to the fact that PCA is encapsulated in the SBEβCD cavity when inclusion compounds are involved.

3.4. DSC analyses for MPEI, MPEI-PCA, MPEI-SBEβCD/PCA conjugates

DSC as analytical technique is also used in monitoring solid state interactions. As indicated in Fig. 5a and b, all studied compounds, except PEI, exhibit a wide endothermic profile in the 50–150 °C range, corresponding to physical dehydration.

Pure PEI shows a characteristic glass transition temperature (T_g) at −57 °C (Fig. 5a). After covering the MNP with PEI polymer, the T_g shifts to seemingly higher temperature domains (−31 °C) (Fig. 5b) and is attributed to the reduction of PEI macromolecules free volume because of significant increase in structural packing capacity. This occurs through charge compensation between negative surface of MNP and positive PEI entities resulted from protonation (confirmed by zeta potentials) and possibly even hydrogen bonding between close PEI chains upon packing. When PCA molecules have interacted with MPEI conjugates, a decrease in the melting point (T_m) from 205 °C (with an

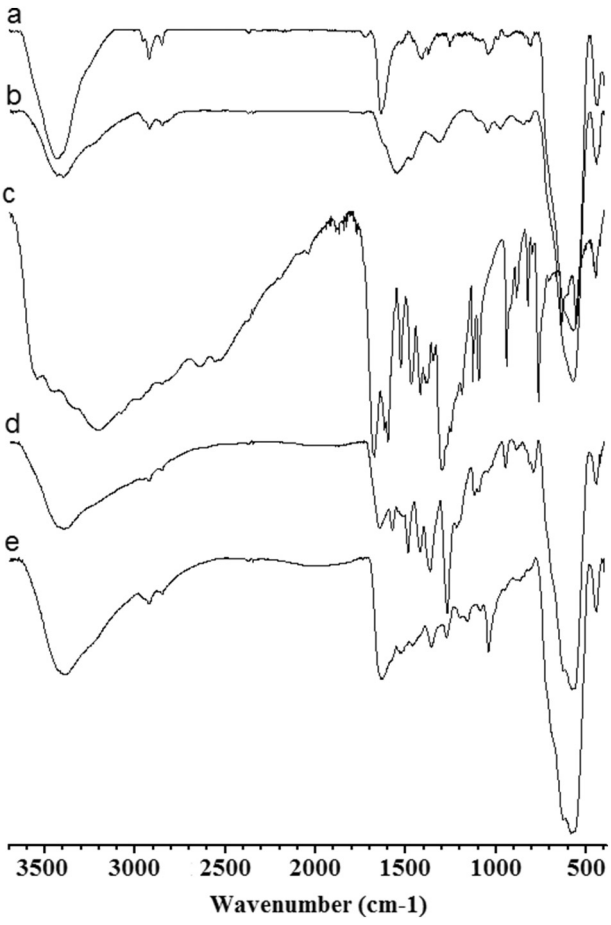

Fig. 4. FT-IR spectra of, (a) MNP, (b) MPEI, (c) PCA, (d) MPEI-PCA, (e) MPEI-SBEβCD/PCA.

enthalpy value of 135.6 J g^{-1}) to 135.6 °C (with an enthalpy value of 10.06 J g^{-1}) was observed. This may be due to the reduction of PCA crystallinity resulted from its acidic dissociation. This process was accompanied by the decreasing of T_g value from −31 °C to −25 °C, indicating a supplementary packing of PEI chains at the nanoconjugate surface. By replacing PCA from MPEI-PCA conjugate with SBEβCD (Fig. 5b), the T_g decreases from −25 °C to −34 °C when the more larger SBEβCD, having the same ionic behaviour as PCA, but hindering the latter's effect sterically generates more free volume between chains. This aspect is reflected in the heating curve of sample MPEI–SBEβCD/PCA where the T_g value is −30 °C, close to −34 °C. It is known that after inclusion complex formation, the guest molecule melting profile either reduces in intensity or disappears [5,21,32]. This is also the case of MPEI–SBEβCD/PCA sample, for which the enthalpy value of the melting profile (4.314 J g^{-1}) greatly reduces compared to that of pure PCA (135.6 J g^{-1}). Regarding PCA in MPEI–PCA sample, the 10.06 J g^{-1} low value indicates a new solid phase formation due to the complexation of the PCA compound [22].

3.5. Entrapment efficiency of PCA or SBEβCD/PCA into MPEIs shell

The entrapment efficiency was calculated using the Eq. (1) [25,26], when the free amount of drug was evaluated by absorbance reading at 287 nm. The results show an MPEI entrapment efficiency of 56% for PCA and 44% for SBEβCD/PCA inclusion complex.

3.6. Nanoparticles morphology

DLS measurements of uncovered MNP in aqueous dispersions showed a hydrodynamic diameter of 480 nm and Zeta Potential values of −24 mV at pH 11 and −1 mV at pH 7, suggesting the decrease of their stability in water when the pH is around physiological one. By covering the MNP with PEI polymer led to an increase in nanoparticle hydrodynamic diameter to 690 nm. This high value is given by the expansion and solvation of the magnetite-attached polymers in water. Zeta Potential measurements indicated a high positive value of +43 mV, which further confirms PEI adsorption on nanoparticles surfaces. Also, this data is an indication of PEI-amine functional groups ionization, which contributes to further MNP-surface polymer expansion due to electrostatic repulsion which amplifies the increase of the hydrodynamic radius. The loading of MPEI with SBEβCD/PCA inclusion complex allowed the embedding of PCA and in this case a lower hydrodynamic diameter (573 nm) than of MPEI (690 nm) was obtained. The decrease of the MPEI-SBEβCD/PCA hydrodynamic diameter is maybe due to the insertion of the inclusion complex, with its solvated $–SO_3^-$ ions, which compensate a part of the positive charges of PEI polycation, diminishing inter- and intra-molecular electrostatic repulsion between PEI chains in water, causing a packing effect. Zeta Potential of the MPEI-SBEβCD/PCA nanoparticles is 40 mV, proving the good dispersion stability in water.

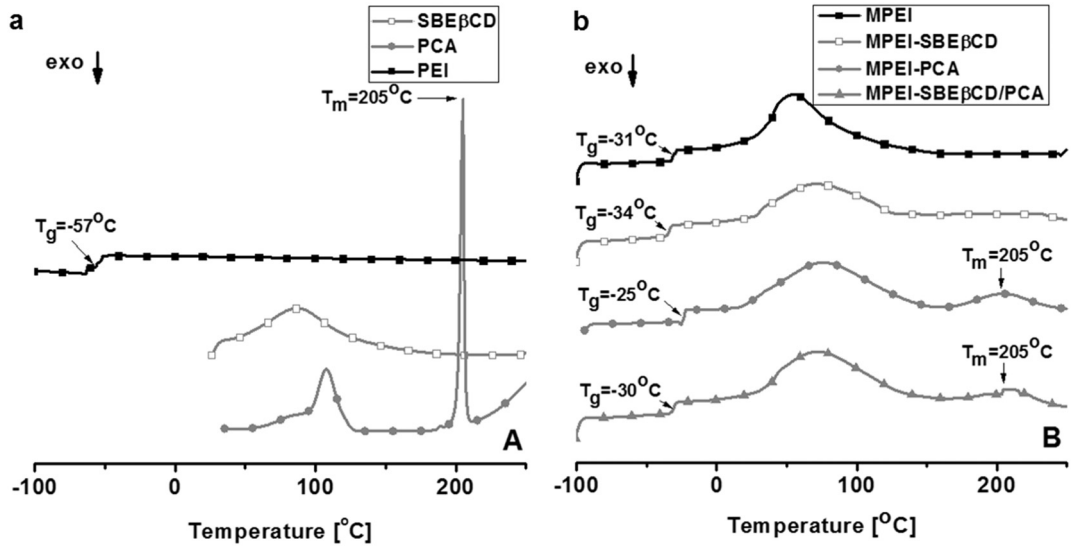

Fig. 5. (a) DSC heating curves of PEI, PCA and SBEβCD in free state; (b) DSC heating curves of MPEI, MPEI-PCA, MPEI-SBEβCD and MPEI-SBEβCD/PCA conjugates.

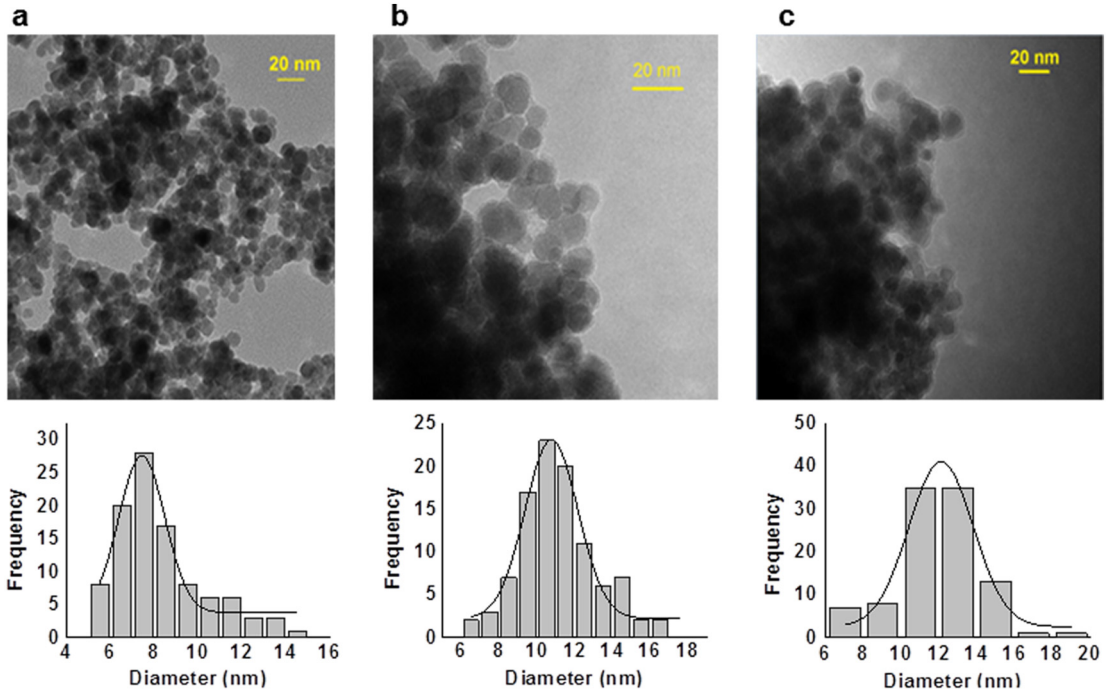

Fig. 6. TEM micrographs and dimensional distribution for: (a) MPEI, (b) MPEI-PCA and (c) MPEI-SBEβCD/PCA conjugates.

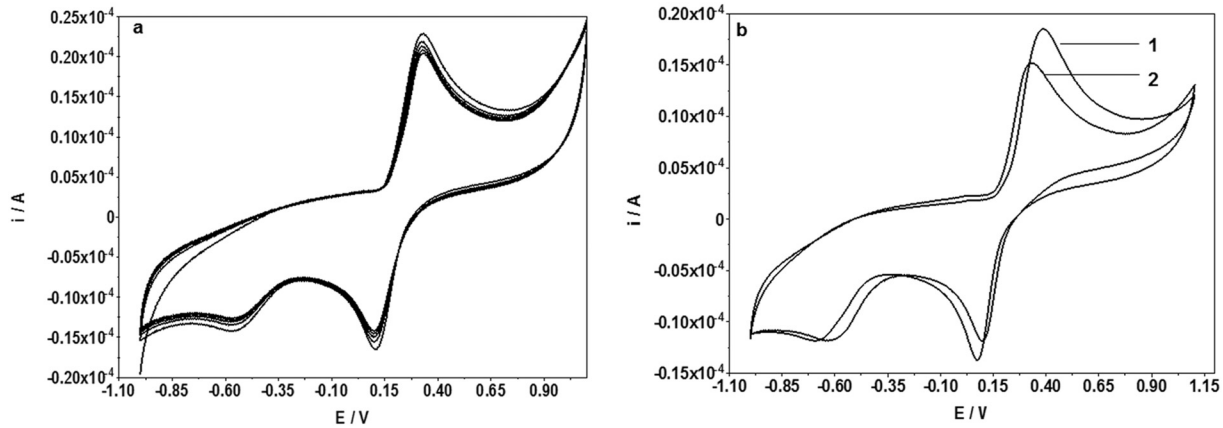

Fig. 7. Redox activity of: (a) PCA 1 mM for 20 successive scans in 0.1 M PBS solution, using a glassy carbon electrode; (b) PCA (curve 1) compared to SBEβCD/PCA 1 mM (curve 2).

The TEM micrographs of the MPEI-PCA and MPEI-SBEβCD/PCA conjugates (Fig. 6) show that the particles are spherical, with an approximate diameter of 10–15 nm and low relative dimensional non-uniformity with aggregation tendency. As measured by DLS method, the dimensions of the nanoparticulate nanoconjugates are larger in comparison with those observed by TEM. The explanation resides in the fact that, during the preparation of TEM samples, the slow evaporation of the solvent concludes with a supplemental contraction of the initially swollen particles and by DLS method the experiments are operated in water solution when PEI chains from the surfaces of nanoparticles intertwine from one particle to the other, resulting into bigger structures.

3.7. Redox properties by electrochemical investigations

Electrochemical characterization was used during the past years in biomedical applications, in food and plant analysis due to its ability to estimate the antioxidant capacity of different compounds. Thanks to the multitude of data published recent years in the field, correlations between structure and function are possible, being reported also relationships between structure and antioxidant capacity [38,39]. The good correlation between the polyphenol structures and the electrochemical properties, explains very well the link between the abundance of the hydroxyl groups and the electronic conjugation. Regarding the literature data, this study highlights how PCA redox properties are affected by its encapsulation in the SBEβCD's cavity or by attaching to the MPEI nanoparticles.

The oxidation of PCA (phenolic compounds with the hydroxyl group in the ortho position) leads to the formation of quinone represented by the single anodic peak at +0.3 V, followed by reversed transformation to initial form through reduction at +0.1 V, as shown by cyclic voltammetry, using a glassy carbon electrode in 0.1 M PBS (Fig. 7a).

The oxidation of PCA (phenolic compounds with the hydroxyl group in the ortho position) on a glassy carbon electrode in 0.1 M PBS leads to the formation of quinone, indicated by the single anodic peak at +0.3 V, followed by reversed transformation to initial form through reduction at +0.15 V, as shown by cyclic voltammetry (Fig. 7a). The results are in agreement with the other studies [40], but in our case the difference between anodic and cathodic peak potential value is much

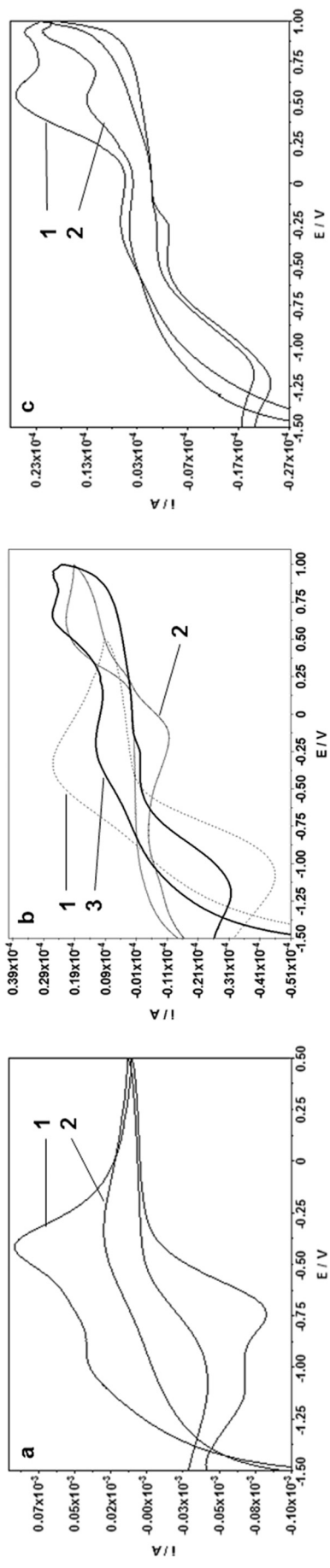

Fig. 8. Cyclic voltammograms of: (a) MNP (curve 1) and MPEI (curve 2); (b) MPEI (curve 1), PCA (curve 2), MPEI-PCA (curve 3); (c) MPEI-PCA (curve 1) MPEI-SBEβCD/PCA (curve 2). The experiments were done in 0.1 M PBS water solution, using carbon screen-printed electrode.

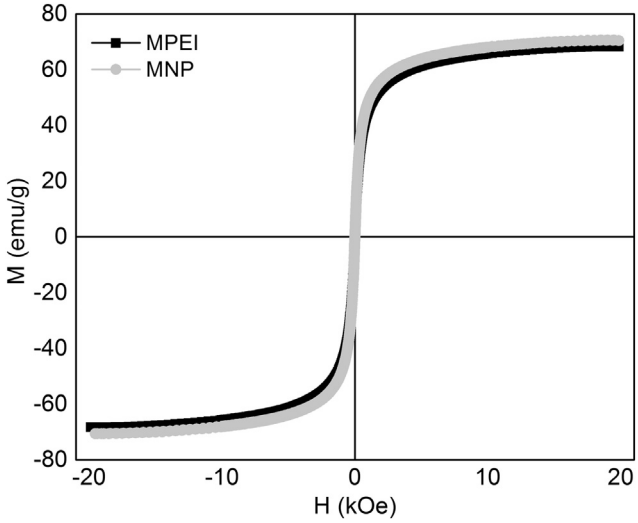

Fig. 9. Magnetization loops of MNP and MPEI nanoparticles.

smaller, which indicates an reversible electrode process, also confirmed by the stable.

By comparing the voltammograms of the SBEβCD/PCA inclusion complex with those of free PCA, (Fig. 7b), several observations can be drawn: (a) the redox behaviour of the SBEβCD/PCA inclusion complex has the same shape of the PCA's cyclic voltammogram showing that the PCA antioxidant activity is maintained even when it is included in the SBEβCD's cavity; (b) the decrease of peaks current intensity indicate that the electronic transfer between PCA and the electrode surface is slightly delayed when it is included in SBEβCD's cavity.

The uncoated MNP voltammograms obtained on a screen-printed carbon electrode reveal redox couple at $-0.4/-0.7$ V due to the Fe^{2+}/Fe^{3+} transformation process (Fig. 8a). The redox peaks of MNP were dramatically diminished when they were covered with PEI polymer caused by the hindered effect of PEI layer over the transition Fe^{2+}/Fe^{3+} (Fig. 8a). By loading MPEI with PCA or SBEβCD/PCA antioxidant species leads to the appearance of the characteristic peaks of the PCA (Fig. 8b,c), proving the redox capacity of the PCA and SBEβCD/PCA when they are loaded into PEI layer.

3.8. Magnetic characterization

Magnetic properties of the dried nanoparticles were analysed using a vibrating-sample magnetometer. Saturation magnetization of uncoated MNP is 70.63 emu/g and 68.37 emu/g in the case of MPEI (Fig. 9). Previously reported results [41] showed a drastically decrease of saturation magnetization values when MNP were covered with polymers. By contrast, in our case, when MNP were covered with PEI polymer the saturation magnetization value is almost constant as compared with uncovered MNP, suggesting the formation of PEI thin layer on MNPs surface [26,42] which is in correlation with TEM results.

The low residual magnetization values (1.05 and 0.91 emu/g for MNP and MPEI respectively) and magnetic coercivity (9.74 and 6.95 Oe for MNP and MPEI respectively) make the hysteresis effect almost unnoticed, giving nanoparticles superparamagnetic properties. The high saturation magnetization values in correlation with superparamagnetic characteristics recommend MPEI core-shell nanoparticles to be used in magnetic guidance in drug delivery applications [12,43].

3.9. Antioxidant activity

The PCA antioxidant property is well known and the results indicate that PCA exerted radical-scavenging action by both mechanisms of donating hydrogen atom and electron [7]. In order to measure free

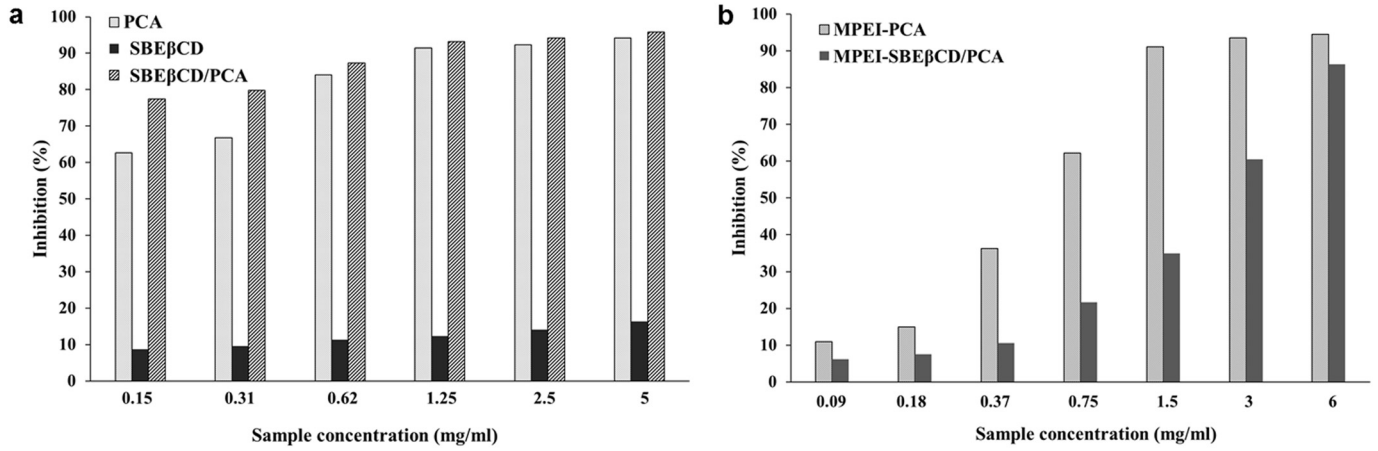

Fig. 10. Antioxidant activity of PCA in different formulations by DPPH method.

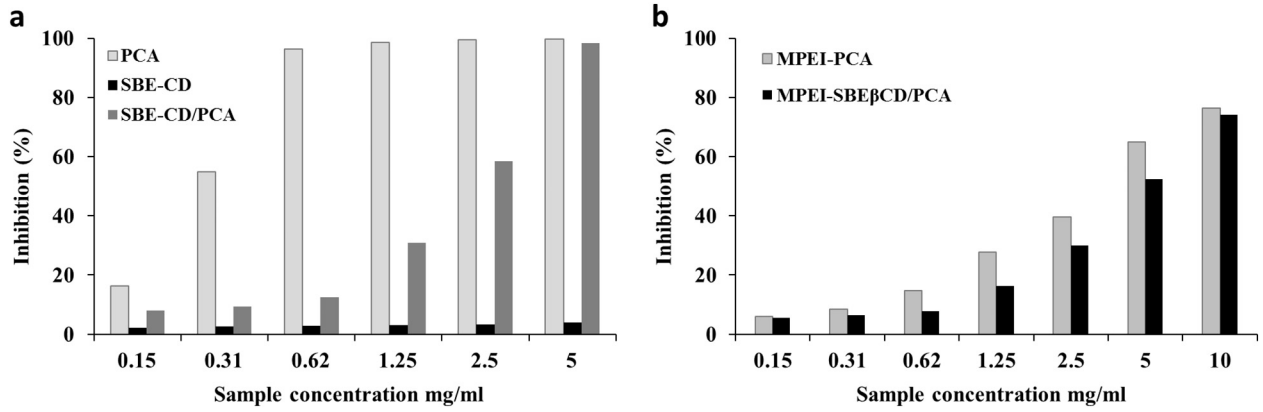

Fig. 11. Antioxidant activity of PCA in different formulations by ABTS method.

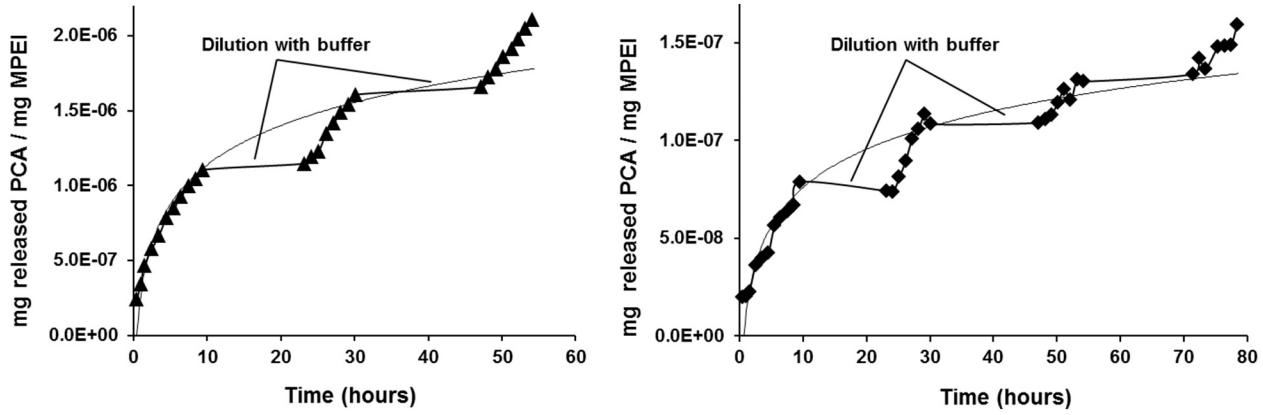

Fig. 12. PCA release profile of (a) MPEI-PCA and (b) MPEI-SBEβCD/PCA nanoconjugates.

radical scavenging activity of free PCA, SBEβCD/PCA inclusion complex, MPEI-PCA and MPEI- SBEβCD/PCA, bleaching property of the DPPH and ABTS radical cation discoloration were used. A freshly prepared DPPH solution exhibits a deep purple colour with an absorption maximum at 517 nm which generally fades when antioxidant molecules reduce DPPH free radicals and convert them into a colourless/bleached product, resulting in a decrease in absorbance at 517 nm band. In the same manner, the discoloration of the ABTS radical cation solution is monitored by measuring the absorbance at 734 nm. Optical absorbance values have permitted to calculate the % of inhibition for each used concentration of antioxidant, applying Eq. (3). Data from Figs. 10 and 11 revealed that the both types of the loaded nanoparticles, containing different formulations of PCA (free form and its inclusion complex), presented radical scavenger properties in different ratios. The DPPH method measures the antioxidant capacity of PCA by a mechanism of donation of a hydrogen radical while the ABTS method through an electron transfer process. The results of the antioxidant activity revealed that SBEβCD and the PEI layer allow the PCA to attend both mechanisms deactivation radicals, as when it is in the free state.

Apparently, the antioxidant capacity of MPEI-PCA is higher than for MPEI-SBEβCD/PCA (Figs. 10b and 11b) but this is explained by the fact that PCA content is higher in MPEI-PCA than in MPEI- SBEβCD/PCA, as demonstrated by entrapping tests (the ratio of PCA in MPEI-PCA to PCA in MPEI-SBEβCD/PCA is 1.28). In this context, the ratio of inhibitions

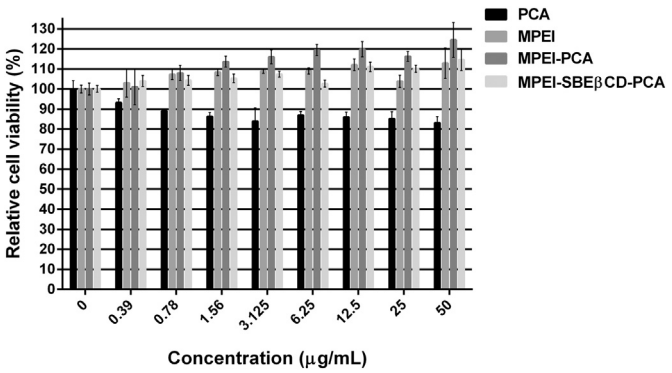

Fig. 13. *In vitro* cytotoxicity assay using MTS method. Relative viabilities of NHDF cells after incubation with MPEI, MPEI-PCA, MPEI-SBEβCD/PCA and control. The results are presented as mean ± standard error from 3 independent experiments performed in triplicate.

between MPEI-PCA and MPEI-SBEβCD/PCA is almost 1.28 in the DPPH assay when the concentration of nanoparticles is at least 6 mg/ml (Fig. 10b), and 1.03 in the ABTS assay when the concentration of nanoparticles is at least 10 mg/ml (Fig. 11b). In the same time for lower concentrations of nanoparticles, MPEI-PCA is more efficient than MPEI-SBEβCD/PCA. This fact can be explained by different loaded formulation of PCA (when PCA is loaded as its free form as compared with its inclusion complex) inducing different entrapment/releasing mechanisms into/from PEI layer.

3.10. Drug release tests

The drug release profiles of MPEI loaded with free PCA and its inclusion complex show a continuous increase on the release rate of PCA from both formulations (MPEI-PCA and MPEI-SBEβCD/PCA) over the course of three days (Fig. 12). This continuous release was obtained after consecutive replacements of the drug-enriched fluid with fresh buffer (see Experimental section). As it can be observed from Fig. 12, the drug release capacity was slower for MPEI-SBEβCD/PCA than for MPEI-PCA, perhaps due to the different formulations of PCA into the two systems, when the electrostatic interactions between PEI shell and PCA or SBEbCD/PCA inclusion complex are different, also giving different release mechanisms. This observation is sustained by the less entrapment ability of MPEIs when were loaded with SBEbCD/PCA rather than free PCA and due to the fact that once the inclusion compound is released from the PEI shell, it should release the PCA from its cavity.

3.11. Cytotoxicity tests (MTS)

The cytotoxicity of the conjugates was tested in parallel with a control using the MTS technique [17] when NHDF cells were cultured in the presence of control, MPEI, MPEI-PCA and MPEI- SBEβCD/PCA conjugates. Fig. 13 presents the calculated cell viability, expressed as an average percentage relative to the control culture (considered 100%), and based on three parallel experiments. No significant differences could be observed in cellular viability after 48 h incubation in the presence of MPEI, MPEI-PCA and MPEI-SBEβCD/PCA conjugates as compare with control sample. The results show no cytotoxic effects of the tested products and the results were in line with previous reported values for other PEI-based nano-particulate systems [44] pointing out the cyto-compatibility of the tested samples as being appropriate for biomedical applications.

4. Conclusions

In this study, the magnetite nanoparticles were synthesized without surfactant and subsequently coated with PEI, resulting MPEI core-shell nanoparticles of 10–15 nm as determined by TEM. The low molecular weight of PEI has been deposited on the surface of magnetite nanoparticles through physical forces facilitating the absorption of PCA antioxidant agent in free form or in its complex with SBEβCD.

The DPPH antioxidant capacity tests and electrochemical studies have shown that the properties of the protocatehuic acid, as natural antioxidant, are not affected by its absorption into the PEI polymer layer nor by its inclusion in the cavity of modified cyclodextrin. The release profile showed that the antioxidant can be released continuously for three days, and the cytotoxicity tests have demonstrated that the conjugates are biocompatible, making them apt for biomedical applications.

Taking into account the low stability of natural antioxidants, the advantages of using PEI coated magnetite nanoparticles has facilitated the loading of PCA as its free form or as its inclusion complex with SBEβCD. It should be emphasized that obtaining conjugates (MPEI, MPEI-PCA, MPEI-SBEβCD/PCA) has been achieved by applying a simple and reproducible method under mild conditions.

In conclusion, by using PEI as a shell of nanoparticles capable of loading inclusion complexes of chemically modified cyclodextrins with anionic groups such as SBEβCD can be a good strategy for using MPEI to load and transport other active principles that are unstable and insoluble in water and last but not least MPEIs are biocompatible and can be guided under the influence of a magnetic field at the desired site.

Acknowledgments

This publication is part of a project that has received funding from the European Union's Horizon 2020 research and innovation programme under grant agreement No 667387 WIDESPREAD 2-2014 SupraChem Lab.

Appendix A. Supplementary data

Supplementary data to this article can be found online at https://doi.org/10.1016/j.msec.2018.10.013.

References

[1] V. Rani, G. Deep, R.K. Singh, K. Palle, U.C. Yadav, Oxidative stress and metabolic disorders: pathogenesis and therapeutic strategies, Life Sci. 148 (2016) 183–193, https://doi.org/10.1016/j.lfs.2016.02.002.
[2] L. Zuo, T. Zhou, B.K. Pannell, A.C. Ziegler, T.M. Best, Biological and physiological role of reactive oxygen species-the good, the bad and the ugly, Acta Physiol. 214 (2015) 329–348, https://doi.org/10.1111/apha.12515.
[3] M.S. Brewer, Natural antioxidants: sources, compounds, mechanisms of action, and potential applications, Compr. Rev. Food Sci. Food Saf. 10 (4) (2011) 221–247, https://doi.org/10.1111/j.1541-4337.2011.00156.x.
[4] W. Wu, Z. Wu, T. Yu, C. Jiang, W.-S. Kim, Recent progress on magnetic iron oxide nanoparticles: synthesis, surface functional strategies and biomedical applications, Sci. Technol. Adv. Mater. 16 (2) (2015) 023501(43pp), https://doi.org/10.1088/1468-6996/16/2/023501.
[5] A. Corciova, C. Ciobanu, A. Poiata, A. Nicolescu, M. Drobota, C.D. Varganici, T. Pinteala, A. Fifere, N. Marangoci, C. Mircea, Inclusion complexes of hesperidin with hydroxypropyl-beta-cyclodextrin. Physico-chemical characterization and biological assessment, Dig. J. Nanomater. Biostrust. 9 (4) (2014) 1623–1637.
[6] X. Ma, Y. Zhao, Biomedical applications of supramolecular systems based on host-guest interactions, Chem. Rev. 115 (15) (2015) 7794–7839, https://doi.org/10.1021/cr500392w.
[7] X. Li, X. Wang, D. Chen, S. Chen, Antioxidant activity and mechanism of protocatechuic acid *in vitro*, Funct. Foods Health Dis. 1 (7) (2011) 232–244.
[8] R. Hao, J. Yu, Z. Ge, L. Zhao, F. Sheng, L. Xu, G. Li, Y. Hou, Developing Fe_3O_4 nanoparticles into an efficient multimodality imaging and therapeutic probe, Nanoscale 5 (2013) 11954–11963, https://doi.org/10.1039/C3NR04157C.
[9] X. Xie, F. Wei, L. Chen, S. Wang, Preparation of molecularly imprinted polymers based on magnetic nanoparticles for the selective extraction of protocatechuic acid from plant extracts, J. Sep. Sci. 38 (2015) 1046–1052, https://doi.org/10.1002/jssc.201401142.
[10] M. Khalkhali, K. Rostamizadeh, S. Sadighian, F. Khoeini, M. Naghibi, M. Hamidi, The impact of polymer coatings on magnetite nanoparticles performance as MRI contrast agents: a comparative study, Daru 23 (45) (2015) 1–12, https://doi.org/10.1186/s40199-015-0124-7.
[11] A.F. Alves, S.G. Mendo, L.P. Ferreira, M.H. Mendonca, P. Ferreira, M. Godinho, M.M. Cruz, M. Deus Carvalho, Gelatine-assisted synthesis of magnetite

nanoparticles for magnetic hyperthermia, J. Nanopart. Res. 18 (27) (2016) 1–13, https://doi.org/10.1007/s11051-016-3327-z.
[12] S. Laurent, A.A. Saei, S. Behzahi, A. Panahifar, M. Mahmoudi, Superparamagnetic iron oxide nanoparticles for delivery of therapeutic agents: opportunities and challenges, Expert Opin. Drug Deliv. 11 (9) (2014) 1449–1470, https://doi.org/10.1517/17425247.2014.924501.
[13] D.S. Ling, T. Hyeon, Chemical design of biocompatible iron oxide nanoparticles for medical applications, Small 9 (9–10) (2013) 1450–1466, https://doi.org/10.1002/smll.201202111.
[14] A. Durdureanu-Angheluta, R. Ardeleanu, M. Pinteala, V. Harabagiu, H. Chiriac, B.C. Simionescu, Silane covered magnetite particles. Preparation and characterisation, Dig. J. Nanomater. Biostruct. 3 (2008) 33–40.
[15] Z.U. Akal, L. Alpsoy, A. Baykal, Superparamagnetic iron oxide conjugated with folic acid and carboxylated quercetin for chemotherapy applications, Ceram. Int. 42 (7) (2016) 9065–9072, https://doi.org/10.1016/j.ceramint.2016.02.166.
[16] A.I. Dascalu, R. Ardeleanu, A. Neamtu, S.S. Maier, C.M. Uritu, A. Nicolescu, M. Silion, D. Peptanariu, M. Calin, M. Pinteala, Transfection-capable polycationic nanovectors which include PEGylated-cyclodextrin structural units: a new synthesis pathway, J. Mater. Chem. B 5 (2017) 7164–7174, https://doi.org/10.1039/C7TB01722G.
[17] R. Ardeleanu, A.I. Dascalu, A. Neamtu, D. Peptanariu, C.M. Uritu, S.S. Maier, A. Nicolescu, B.C. Simionescu, M. Barboiu, M. Pinteala, Multivalent polyrotaxane vectors as adaptive cargo complexes for gene therapy, Polym. Chem. 9 (2018) 845–859, https://doi.org/10.1039/c7py01256j.
[18] A. Durdureanu-Angheluta, M.-E. Ignat, S.S. Maier, L. Pricop, A. Coroaba, A. Fifere, M. Pinteala, A. Chiriac, Lipolytic biocatalyst based on recyclable magnetite-polysiloxane nanoparticles, Appl. Surf. Sci. 292 (2014) 898–905, https://doi.org/10.1016/j.apsusc.2013.12.077.
[19] A. Durdureanu-Angheluta, A. Dascalu, A. Fifere, A. Coroaba, L. Pricop, H. Chiriac, V. Tura, M. Pinteala, B.C. Simionescu, Progress in the synthesis and characterization of magnetite nanoparticles with amino groups on the surface, J. Magn. Magn. Mater. 324 (2012) 1679–1689, https://doi.org/10.1016/j.jmmm.2011.11.062.
[20] L. Pricop, A. Durdureanu-Angheluta, M. Spulber, I. Stoica, A. Fifere, N.L. Marangoci, A.I. Dascalu, R. Tigoianu, V. Harabagiu, M. Pinteala, B.C. Simionescu, Synthesis and micellization of polydimethylsiloxane-carboxy terminated poly(ethylene oxide) graft copolymer in aqueous and organic media and its application for synthesis of core-shell magnetic particles, E-Polymers 093 (2010) 1–19.
[21] A. Corciova, C. Ciobanu, A. Poiata, C. Mircea, A. Nicolescu, M. Drobota, C.D. Varganici, T. Pinteala, N. Marangoci, Antibacterial and antioxidant properties of hesperidin: beta-cyclodextrin complexes obtained by different techniques, J. Incl. Phenom. Macrocycl. Chem. 81 (1–2) (2015) 71–84, https://doi.org/10.1007/s10847-014-0434-2.
[22] B. Minea, N. Marangoci, D. Peptanariu, I. Rosca, V. Nastasa, A. Corciova, C. Varganici, A. Nicolescu, A. Fifere, A. Neamtu, M. Mares, M. Barboiu, M. Pinteala, Inclusion complexes of propiconazole nitrate with substituted β cyclodextrins:the synthesis and *in silico* and *in vitro* assessment of their antifungal properties, New J. Chem. 40 (2) (2016) 1765–1776, https://doi.org/10.1039/C5NJ01811K.
[23] R. Massart, Preparation of aqueous magnetic liquids in alkaline and acidic media, IEEE Trans. Magn. 17 (2) (1981) 1247–1248, https://doi.org/10.1109/TMAG.1981.1061188.
[24] A. Durdureanu-Angheluta, L. Pricop, I. Stoica, C.A. Peptu, A. Dascalu, N. Marangoci, F. Doroftei, H. Chiriac, M. Pinteala, B.C. Simionescu, Synthesis and characterization of magnetite particles covered with α-trietoxysilil-polydimethylsiloxane, J. Magn. Magn. Mater. 322 (19) (2010) 2956–2968, https://doi.org/10.1016/j.jmmm.2010.05.013.
[25] M.K. Forrest, F.Y. Wang, C. Fang, H. Mok, K. Wang, J.R. Silber, R.G. Ellenbogen, M. Zhang, Doxorubicin loaded iron oxide nanoparticles overcome multidrug resistance in cancer *in vitro*, J. Control. Release 152 (1) (2011) 76–83, https://doi.org/10.1016/j.jconrel.2011.01.024.
[26] M. Khalkhali, S. Sadighian, K. Rostamizadeh, F. Khoeini, M. Naghibi, N. Bayat, M. Habibizadeh, M. Hamidi, Synthesis and characterization of dextran coated magnetite nanoparticles for diagnostics and therapy, Bioimpacts 5 (3) (2015) 141–150, https://doi.org/10.15171/bi.2015.19.
[27] X. Hua, S. Tan, H.M.H.N. Bandara, Y. Fu, S. Liu, H.D.C. Smyth, Externally controlled triggered-release of Drug from PLGA micro and nanoparticles, PLoS One 9 (12) (2014) e114271, , https://doi.org/10.1371/journal.pone.0114271.
[28] S.T. Shah, W.A. Yehye, O. Saad, K. Simarani, Z.Z. Chowdhury, A.A. Alhadi, L.A. Al-Ani, Surface functionalization of iron oxide nanoparticles with gallic acid as potential antioxidant and antimicrobial agents, Nano 7 (10) (2017) 306, https://doi.org/10.3390/nano7100306.
[29] R. Re, N. Pellegrini, A. Proteggente, A. Pannala, M. Yang, C. Rice-Evans, Antioxidant activity applying an improved ABTS radical cation decolorization assay, Free Radic. Biol. Med. 26 (1999) 1231–1237, https://doi.org/10.1016/S0891-5849(98)00315-3.
[30] R. Deng, Y. Yue, F. Jin, Y. Chen, H.-F. Kung, M.C.M. Lin, C. Wu, Revisit the complexation of PEI and DNA - how to make low cytotoxic and highly efficient PEI gene transfection non-viral vectors with a controllable chain length and structure? J. Control. Release 140 (1) (2009) 40–46, https://doi.org/10.1016/j.jconrel.2009.07.009.
[31] A. Fifere, N. Marangoci, S. Maier, A. Coroaba, D. Maftei, M. Pinteala, Theoretical study on β-cyclodextrin inclusion complexes with propiconazole and protonated propiconazole, Beilstein J. Org. Chem. 8 (2012) 2191–2201, https://doi.org/10.3762/bjoc.8.247.
[32] N. Marangoci, M. Mares, M. Silion, A. Fifere, C. Varganici, A. Nicolescu, C. Deleanu, A. Coroaba, M. Pinteala, B.C. Simionescu, Inclusion complex of a new propiconazole derivative with β-cyclodextrin: NMR, ESI–MS and preliminary pharmacological studies, Res. Pharm. Sci. 1 (1) (2011) 27–37, https://doi.org/10.1016/j.rinphs.2011.07.001.
[33] H.E. Grandelli, B. Stickle, A. Whittington, E. Kiran, Inclusion complex formation of β-cyclodextrin and naproxen: a study on exothermic complex formation by differential scanning calorimetry, J. Incl. Phenom. Macrocycl. Chem. 77 (1–4) (2013) 269–277, https://doi.org/10.1007/s10847-012-0241-6.
[34] A.C.H. Barreto, V.R. Santiago, R.M. Freire, S.E. Mazzetto, J.C. Denardin, G. Mele, I.M. Cavalcante, M.E.N.P. Ribeiro, N.M.P.S. Ricardo, T. Goncalves, L. Carbone, T.L.G. Lemos, O.D.L. Pessoa, P.B.A. Fechine, Magnetic nanosystem for cancer therapy using oncocalyxone a, an antitomour secondary metabolite isolated from a Brazilian plant, Int. J. Mol. Sci. 14 (9) (2013) 18269–18283, https://doi.org/10.3390/ijms140918269.
[35] A. Akbarzadeh, N. Zarghami, H. Mikaeili, D. Asgari, A.M. Goganian, H.K. Khiabani, M. Samiei, S. Davaran, Synthesis, characterization, and *in vitro* evaluation of novel polymer-coated magnetic nanoparticles for controlled delivery of doxorubicin, Nanotechnol. Sci. Appl. 5 (2012) 13–25, https://doi.org/10.2147/NSA.S24328.
[36] S.U. Muhammad, H.M. Mohd, A.U. Kura, F. Sharida, M.J. Mas, F.A.S. Fathinul, Synthesis and characterization of protocatechuic acid-loaded gadolinium-layered double hydroxide and gold nanocomposite for theranostic application, Appl. Nanosci. (2018) 1–14, https://doi.org/10.1007/s13204-018-0752-6.
[37] I.A. Jankovic, Z.V. Saponjic, E.S. Dzunuzovic, J.M. Nedeljkovic, New hybrid properties of TiO_2 nanoparticles surface modified with catecholate type ligands, Nanoscale Res. Lett. 5 (2009) 81–89, https://doi.org/10.1007/s11671-009-9447-y.
[38] R.D. O'Neill, J.P. Lowry, M. Mas, Monitoring brain chemistry *in vivo*: voltammetric techniques, sensors, and behavioral applications, Crit. Rev. Neurobiol. 12 (1–2) (1998) 69–127, https://doi.org/10.1615/CritRevNeurobiol.v12.i1-2.40.
[39] M. Born, P.A. Carrupt, R. Zini, F. Bree, J.P. Tillement, K. Hostettmann, B. Testa, Electrochemical behaviour and antioxidant activity of some natural polyphenols, Helv. Chim. Acta 79 (4) (1996) 1147–1158, https://doi.org/10.1002/hlca.19960790422.
[40] A. Simic, D. Manojlovic, D. Segan, M. Todorovic, Electrochemical behavior and antioxidant and prooxidant activity of natural phenolics, Molecules 12 (10) (2007) 2327–2340, https://doi.org/10.3390/12102327.
[41] Z. Shaterabadi, G. Nabiyouni, M. Soleymani, High impact of *in situ* dextran coating on biocompatibility, stability and magnetic properties of iron oxide nanoparticles, Mater. Sci. Eng. C 75 (2017) 947–956, https://doi.org/10.1016/j.msec.2017.02.143.
[42] A.G. Kolhatkar, A.C. Jamison, D. Litvinov, R.C. Willson, T.R. Lee, Tuning the magnetic properties of nanoparticles, Int. J. Mol. Sci. 14 (8) (2013) 15977–16009, https://doi.org/10.3390/ijms140815977.
[43] J.L. Viota, A. Carazo, J.A. Munoz-Gamez, K. Rudzka, R. Gomez-Sotomayor, A. Ruiz-Extremera, J. Salmeron, A.V. Delgado, Functionalized magnetic nanoparticles as vehicles for the delivery of the antitumor drug gemcitabine to tumor cells. Physicochemical in vitro evaluation, Mater. Sci. Eng. C 33 (3) (2013) 1183–1192, https://doi.org/10.1016/j.msec.2012.12.009.
[44] C.M. Uritu, M. Calin, S.S. Maier, C. Cojocaru, A. Nicolescu, D. Peptanariu, C.A. Constantinescu, D. Stan, M. Barboiu, M. Pinteala, Flexible cyclic siloxane core enhances the transfection efficiency of polyethylenimine-based non-viral gene vectors, J. Mater. Chem. B 3 (42) (2015) 8250–8267, https://doi.org/10.1039/C5TB01342A.